Interlayer-state-driven superconductivity in CaC_6 studied by angle-resolved photoemission spectroscopy

Wonshik Kyung,[1] Yeongkwan Kim,[1,2] Garam Han,[1] Choonshik Leem,[1] Chul Kim,[1] Yoonyoung Koh,[1] Beomyoung Kim,[1] Youngwook Kim,[3] Jun Sung Kim,[3] Keun Su Kim,[2,3,4] Eli Rotenberg,[2] Jonathan D. Denlinger,[2] and Changyoung Kim[1,*]

[1]*Institute of Physics and Applied Physics, Yonsei University, Seoul 120-749, Korea*

[2]*Advanced Light Source, Lawrence Berkeley National Laboratory, California 94720, USA*

[3]*Department of Physics, Pohang University of Science and Technology, Pohang 790-784, Korea*

[4]*Center for Artificial Low-Dimensional Electronic Systems, Institute for Basic Science, Pohang 790-784, Korea*

(Received 16 September 2014; revised manuscript received 21 October 2015; published 30 December 2015)

We performed angle-resolved photoemission experiments on CaC_6 and measured k_z-dependent electronic structures to investigate the interlayer states. The results reveal a spherical interlayer Fermi surface centered at the Γ point. We also find that the graphene-driven band possesses a weak k_z dispersion. The overall electronic structure shows a peculiar single-graphene-layer periodicity in the k_z direction although the CaC_6 unit cell is supposed to contain three graphene layers. This suggests that the *c*-axis ordering of Ca has little effect on the electronic structure of CaC_6. In addition to CaC_6, we also studied the a low-temperature superconductor BaC_6. For BaC_6, the graphene-band Dirac-point energy is smaller than that of CaC_6. Based on data from CaC_6 and BaC_6, we rule out the C_{xy} phonon mode as the origin of the superconductivity in CaC_6, which strongly suggests interlayer-state-driven superconductivity.

DOI: 10.1103/PhysRevB.92.224516 PACS number(s): 74.25.Jb, 71.18.+y, 71.20.−b, 79.60.Fr

Since the discovery of superconductivity in CaC_6 [1], a graphite intercalation compound (GIC) with the highest transition temperature, there have been various reports that suggest different origins for the superconductivity. The true origin of the superconductivity is still under debate. There were two prevailing views on the superconducting mechanism: The first view is the interlayer-state-driven (IL-state-driven) superconductivity that emphasizes the role of IL states in the superconductivity [2–8]. The other is the graphene-driven superconductivity, which is equivalent to the electron-doped graphite-based superconductivity [9,10].

Various experiments have been performed to find the origin of the superconductivity [5,6,9–17], including angle-resolved photoemission spectroscopy (ARPES) experiments for electronic structure studies [6,9,10,16,17]. IL states are indeed observed, which is consistent with the IL-driven superconductivity [6,16,17]. More importantly, there is a report that shows a superconducting gap only on the IL Fermi surface but not on the graphene π^* band [6]. It was argued in the report that the role of IL states is more important than that of the graphene band in the formation of Cooper pairs. On the other hand, there are other reports of ARPES results that suggest a significant role of the graphene π^* bands [9,10]. In fact, there was no sign of the IL band in these reports. In addition, superconducting transition temperatures of various superconducting GICs could be successfully estimated by using electron-phonon coupling constants extracted from the graphene in-plane phonon-related kink structures.

There are conflicting reports, as discussed above, even for the basic electronic structure. Part of the reason comes from the absence of full Brillouin zone (BZ) electronic structure data. Because the IL band is expected to have three-dimensional (3D) dispersion, k_z-dependent electronic-structure studies are essential. However, to the best of our knowledge, no report exists of k_z-dependent data that cover the full BZ. In this case, the use of inappropriate photon energies (k_z being at a wrong place in the BZ) could result in the absence of an IL band in the data. For these reasons, we performed photon-energy-dependent high-resolution ARPES studies to map out the full 3D electronic structure of CaC_6. In addition, we also investigated a low-temperature superconductor BaC_6 ($T_c = 65$ mK) [18] for a comparative study. From our results, we not only confirm the existence of the IL band but also discover a peculiar k_z periodicity in CaC_6. Furthermore, the measured electronic structure of BaC_6 supports the interlayer-state-driven superconductivity scenario.

CaC_6 samples were prepared via immersion of natural single-crystalline graphite in a Li-Ca alloy for 14 days [11,19]. Magnetic susceptibility measurements revealed sharp ($\Delta T < 0.3$ K) superconducting transitions at 11.6 K. In addition, BaC_6 was synthesized by using the vapor-reaction method at 450 °C for six weeks. All samples were prepared in an Ar-filled glove box and cleaved at 30 K in an ultrahigh vacuum better than 8×10^{-11} torr. ARPES experiments were performed with Scienta R4000 and R8000 electron spectrometers operating at beam lines 7.0.1 and 4.0.3, respectively, of the Advanced Light Source.

Before going into the experimental results, we first discuss the crystal structure of CaC_6. Due to the symmetry change imposed by the intercalated Ca, the CaC_6 structure has a rhombohedron unit cell belonging to the $R\bar{3}m$ space group ($A\alpha A\beta A\gamma$ stacking) as shown in Fig. 1(a). It thus has a three-times-smaller Brillouin zone (BZ) compared with that of graphene [Fig. 1(b)]. This can cause a possible confusion between the IL band and folded graphene band located at the Γ point. Fortunately, the two bands have different k_z behavior and we can distinguish them based on the k_z dependence.

*Present address: Department of Physics and Astronomy, Seoul National University, Seoul 08826, Korea; changyoung@snu.ac.kr

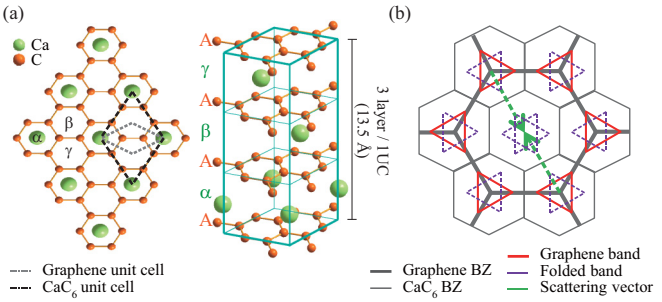

FIG. 1. (Color online) (a) CaC_6 unit cell. In-plane unit cell (left) and three-dimensional unit cell (right). Ca and C atoms are in green and orange, respectively. Gray and black dashed lines show the in-plane unit cell of graphene and CaC_6, respectively. (b) CaC_6 Brillouin zone (BZ) with a $\sqrt{3} \times \sqrt{3}$ scattering due to the three-times larger unit-cell size of CaC_6 compared to that of graphene. Thick and thin gray lines indicate BZs of graphene and CaC_6, respectively. Solid red and dashed purple triangles indicate graphene π^* bands and its replica from the $\sqrt{3} \times \sqrt{3}$ scattering.

Figure 2 represents the band structure of CaC_6 taken along the Γ-K direction [20]. Although the overall Fermi surface topology follows the graphene case, there are two distinct features compared with previous reports [6,9,17]. The first one is a weak circular feature at the center of the graphene BZ. The other feature is a linear Fermi surface segment (indicated by the red arrow) that connects the triangular graphene Fermi surface pockets at K and K'. We first discuss the circular pocket at the Γ and then discuss the extra line segment later.

The character of the weak circular pocket at the Γ point can be the folded graphene or IL bands. In order to investigate the character of the circular pocket at Γ, we explore the k_z dependence of the electronic structure. Figure 3(a) shows a k_z-dependent Γ-K cut at the Fermi energy along the Γ-M direction [20]. The grid lines represent high-symmetry lines of the BZ. Note that, for simplicity, k_x and k_z in Figs. 3(a) and 3(b) are expressed in different units: in units of $4\pi/3a$ (graphene unit cell) for k_x and π/c (single graphene layer unit cell,

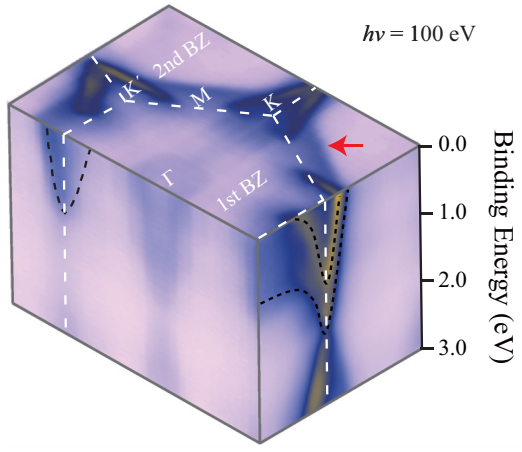

FIG. 2. (Color online) Fermi surfaces of CaC_6 taken with a photon energy of 100 eV. White dashed lines represent the graphene BZ, not CaC_6. The red arrow indicates a Fermi surface line segment from an extra band.

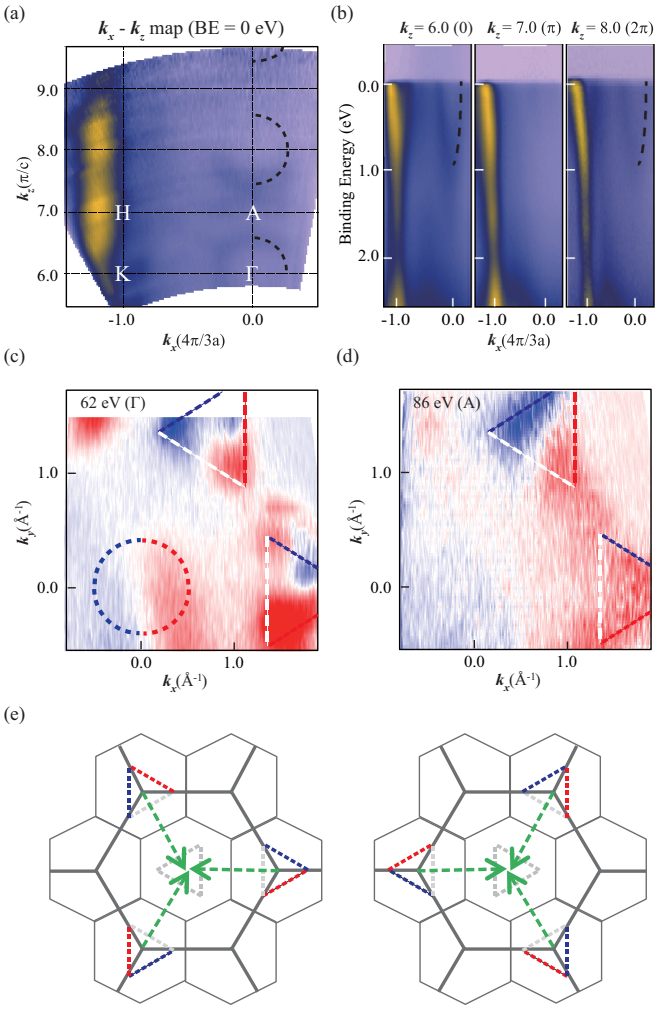

FIG. 3. (Color online) (a) k_x-k_z map along the Γ-K symmetry line. The dashed black half circle indicates the spherical IL Fermi surface. (b) ARPES data along the Γ-K direction for the three k_z values of $0, \pi, 2\pi$. (c), (d) Two Fermi surfaces measured with circular dichroism method at 62 eV (Γ) and 86 eV (A), respectively. The dashed circle and triangle indicate the locations of IL and graphene π^* states, respectively. The expected circular dichroism pattern is shown by the color of the lines. (e) Dichroism pattern of the graphene band near the Γ point in the presence of a $\sqrt{3} \times \sqrt{3}$ scattering. Thick and thin gray lines mean BZs of graphene and of CaC_6, respectively.

(4.52 Å)/(1 uc) for k_z. Based on our data, the inner-potential value for CaC_6 is 17 eV with the $k_z = 0$ points located at 17, 54, 105, 171 eV [$k_z = 4, 6, 8, 10$ (π/c), respectively].

The k_x-k_z map in Fig. 3(a) shows clear spherical Fermi surfaces periodically located around Γ points. Figure 3(b) shows ARPES data taken at three different k_z values of 6, 7, and 8 [corresponding to horizontal cuts in Fig. 3(a)]. A weak parabolic feature clearly appears and disappears near the Γ point for different k_z points (indicated by the dashed line). Such k_z-dispersive behavior strongly suggests that the circular pocket at the Γ point comes from the IL band because the graphene π^* band is expected to have no or very weak k_z dispersion. The maximum binding energy of the IL band is about 0.85 eV. As for the size of the Fermi surface pocket, the

measured diameter is 0.82 $Å^{-1}$ which is quite a bit smaller than the recently reported experimental value [17], but comparable to the theoretically calculated value [7,21]. The reason for the discrepancy may come from their use of a low photon energy [17], at which estimation and comparison of the true Fermi-surface size compared to the BZ, the size can be rather different because the full BZ cannot be measured.

We may verify the character of the circular feature in another way. Circular dichroism (CD) ARPES is found to be sensitive to orbital characteristics [22–24] and therefore can be used to analyze the constituting orbitals. Figures 3(c) and 3(d) show two Fermi-surface maps taken at the Γ (62 eV) and A (86 eV) points. For both Fermi-surface maps, graphene π^* bands around the K points have their unique CD pattern. As for the circular feature at the center of the BZ, a CD pattern with a vertical node is seen for the data taken at Γ while there is no CD for the data taken at the A point. If the circular feature stems from $\sqrt{3} \times \sqrt{3}$ folded graphene bands, the CD pattern should be averaged out, as illustrated in Fig. 3(e). We then expect no CD signal for both Γ and A. This is not the case, as shown in Figs. 3(c) and 3(d). Therefore, it is likely that the IL band is responsible for the circular feature. It appears that the CD signal originates from the partial Ca 3d character in the IL band [3,25].

We now move our discussion to the extra linear segment in Fig. 2 indicated by the red arrow. We believe the linear segment in the Fermi surfaces originates from the graphene π^* state because the feature appears only in the second BZ, but not in the first BZ. Such behavior is reminiscent of the pseudo spin effect of the triangular graphene Fermi-surface pocket [26]. Note that the triangular Fermi-surface pocket also has no spectral weight in the first BZ, as seen in Fig. 2. To further investigate the origin of the segment, we did k_z-dependent ARPES measurements along the K-M high-symmetry cut. Figures 4(a) and 4(b) show k_x-k_z maps at 0 and 1 eV binding energies, respectively. Although the k_z-dependent signature is very weak in Fig. 4(a), we can find a clear dispersive signature in the 1-eV data in Fig. 4(b).

K-M-K and H-L-H high-symmetry-cut data in Figs. 4(c) and 4(d) provide more information. As can be seen from the ARPES data in Figs. 4(c) and 4(d), CaC_6 has two bands near the K (H) points. The upper band has a strong intensity with the band bottom at 1.16 eV while the lower band is weak with the band bottom at 1.99 eV. The overall k_z-dependent behavior of the bands is similar to that of the graphite bands, and the origin of such band structure is believed to come from partial hybridization between the IL and π^* bands [4,21]. Looking at more details, the upper band is k_z independent and produces the triangular graphene Fermi surface in Fig. 2. On the other hand, the lower weak band produces the circular shape k_z-dependent signature in Fig. 4(b) (dashed red line). It is also responsible for the linear Fermi-surface segment in Fig. 2.

As discussed above, we observed k_z dispersions not only in the IL band but also in the graphene band. A peculiar aspect of the observation is that both IL and graphene π^* states possess a single-graphene-layer periodicity (4.52 Å) in the z direction despite the fact that the CaC_6 unit cell contains three graphene layers (13.56 Å). These observations can be understood if we consider that c-axis Ca ordering has little effect on overall electronic structure.

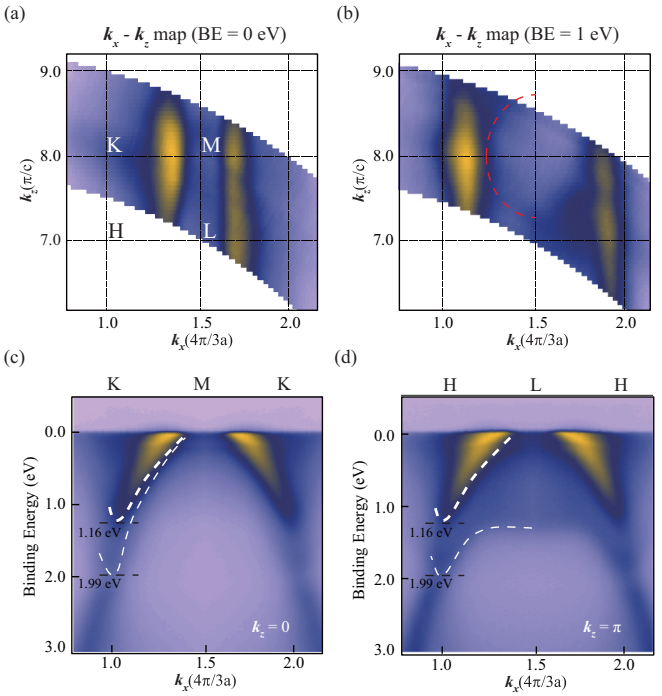

FIG. 4. (Color online) k_x-k_z maps along the M-K cut at binding energies of (a) 0 eV and (b) 1 eV. Thin dotted black lines indicate high-symmetry lines. Thick dashed red line in panel (b) shows the k_z dispersion of the extra π^* band. ARPES data along (c) K-M-K (k_z = 0) and (d) H-L-H ($k_z = \pi$) directions, respectively. White thick and thin dashed lines mark the upper and lower bands, respectively.

The next step is to find the connection between the experimentally observed electronic structure and the superconductivity. Since CaC_6 is believed to be a BCS superconductor [11,27], we need to consider the electron-phonon coupling. Calculation of the Eliashberg function shows that three phonon modes can mediate the pairing: intercalant in-plane (I_{xy}), graphene out-of-plane (C_z), and graphene in-plane (C_{xy}) phonon modes [21,28]. Among the three phonon modes, I_{xy} and C_z require IL-state electrons while C_{xy} need graphene π^*-state electrons. Our experimental data with both IL and

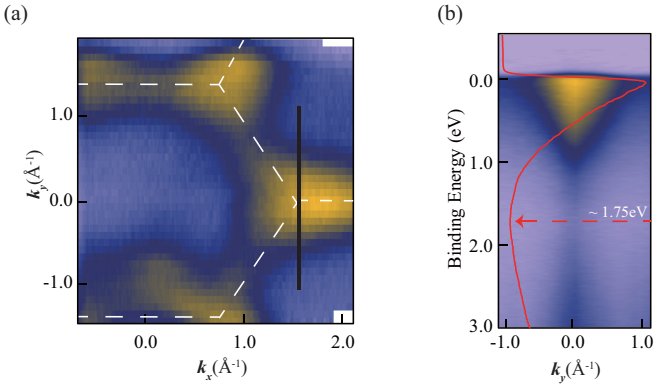

FIG. 5. (Color online) (a) Fermi surface of BaC_6 at k_z = 0 (130 eV). White dashed lines represent the graphene BZs. (b) ARPES data along the black line in panel (a). The red curve represents the integrated density of states, and the arrow marks E_D (~1.75 eV).

TABLE I. Superconducting transition temperature (T_c), E_D, and carbon in-plane phonon-mode energies (C_{xy}) of CaC_6, KC_8, and BaC_6

	CaC_6	KC_8	BaC_6
T_c (K)	11.5	0.39	0.065
E_D (eV)	1.99	1.35	1.75
C_{xy} - Raman (eV) [12]	0.187		0.187
C_{xy} - ARPES (eV) [9,10]	0.165	0.165	

graphene bands seem to allow all three phonon modes to be the pairing glue.

However, we can count out the C_{xy}-driven superconductivity scenario based on the data from BaC_6 in Fig. 5. Here, we compare the amounts of the electron doping in graphene layers for CaC_6, BaC_6, and KC_8 [10]. Figure 5(b) shows that the binding energy of the Dirac point (E_D) for nonsuperconducting BaC_6 (1.75 eV) is smaller than that for CaC_6 (1.99 eV) [29]. It is also known that E_D of the superconducting KC_8 (T_c = 0.39 K) is located at 1.35 eV [10]. On the other hand, several Raman and ARPES results show intercalant-independent C_{xy} phonon-mode energies in various GICs, as shown in Table I [9,10,12].

The main parameter for the McMillan formula [30] for the BCS superconductivity is the electron-phonon coupling (EPC). From Eliashberg theory, we know that the EPC constant λ is proportional to the square of electron-phonon coupling strength g and electron density of states at the Fermi energy. In addition, g is related to the phonon-mode energy and Bloch wave function [31]. As noted earlier, various superconducting GICs share a similar C_{xy} phonon-mode energy. We can then assume a similar g value for various alkali-metal intercalated GICs since their electronic structures are similar. Therefore, the amount of electron transfer to the graphene layer should be the main parameter to the C_{xy} phonon mode driven superconductivity. We note that BaC_6, which has more electrons in the graphene layer than KC_8, has a lower superconducting-transition temperature than KC_8. Therefore, the C_{xy}-driven-superconductivity scenario fails to consistently account for the superconductivity in GICs. This fact excludes the possibility for C_{xy}-phonon-driven superconductivity, which suggests an IL-state-driven superconductivity.

In conclusion, we measured k_z-dependent electronic structures of CaC_6 by using ARPES to investigate the IL states. We observe a k_z-dispersive IL band and two split carbon bands. All the bands show a periodicity of a single graphene layer. Comparison of our data from BaC_6 with those from CaC_6 as well as with published KC_8 data allows us to rule out the C_{xy} phonon mode as the origin of the superconductivity. Therefore, the origin of the superconductivity in CaC_6 is either the Ca_{xy} or the C_z phonon mode, both of which point to IL-driven superconductivity.

We are grateful to J. Yu for fruitful discussions. This research was supported by the Global Research Laboratory (2011-00329) through the National Research Foundation of Korea (NRF) funded by the Ministry of Science, ICT (Information and Communication Technologies) and Future Planning and the Converging Research Center Program through the Ministry of Science, ICT and Future Planning, Korea (2014M3C1A8053752), the Mid-Career Researcher Program (Grant No. 2012-013838) and SRC Center for Topological Matter (Grant No. 2011-0030046).

[1] T. E. Weller, M. Ellerby, S. S. Saxena, R. P. Smith, and N. T. Skipper, Nat. Phys. **1**, 39 (2005).
[2] G. Csanyi, P. B. Littlewood, A. H. Nevidomskyy, C. J. Pickard, and B. D. Simons, Nat. Phys. **1**, 42 (2005).
[3] I. I. Mazin, Phys. Rev. Lett. **95**, 227001 (2005).
[4] I. I. Mazin, L. Boeri, O. V. Dolgov, A. A. Golubov, G. B. Bachelet, M. Giantomassi, and O. K. Andersen, Physica C **460-462**, 116 (2007).
[5] D. G. Hinks, D. Rosenmann, H. Claus, M. S. Bailey, and J. D. Jorgensen, Phys. Rev. B **75**, 014509 (2007).
[6] K. Sugawara, T. Sato, and T. Takahashi, Nat. Phys. **5**, 40 (2009).
[7] A. Sanna, G. Profeta, A. Floris, A. Marini, E. K. U. Gross, and S. Massidda, Phys. Rev. B **75**, 020511(R) (2007).
[8] G. Profeta, M. Calandra, and F. Mauri, Nat. Phys. **8**, 131 (2012).
[9] T. Valla, J. Camacho, Z.-H. Pan, A. V. Fedorov, A. C. Walters, C. A. Howard, and M. Ellerby, Phys. Rev. Lett. **102**, 107007 (2009).
[10] Z.-H. Pan, J. Camacho, M. H. Upton, A. V. Fedorov, C. A. Howard, M. Ellerby, and T. Valla, Phys. Rev. Lett. **106**, 187002 (2011).
[11] J. S. Kim, R. K. Kremer, L. Boeri, and F. S. Razavi, Phys. Rev. Lett. **96**, 217002 (2006).
[12] M. P. M. Dean, C. A. Howard, S. S. Saxena, and M. Ellerby, Phys. Rev. B **81**, 045405 (2010).
[13] R. S. Gonnelli, D. Daghero, D. Delaude, M. Tortello, G. A. Ummarino, V. A. Stepanov, J. S. Kim, R. K. Kremer, A. Sanna, G. Profeta, and S. Massidda, Phys. Rev. Lett. **100**, 207004 (2008).
[14] J. S. Kim, L. Boeri, R. K. Kremer, and F. S. Razavi, Phys. Rev. B **74**, 214513 (2006).
[15] K. C. Rahnejat, C. A. Howard, N. E. Shuttleworth, S. R. Schofield, K. Iwaya, C. F. Hirjibehedin, Ch. Renner, G. Aeppli, and M. Ellerby, Nat. Commun. **2**, 558 (2011).
[16] K. Kanetani, K. Sugawara, T. Sato, R. Shimizu, K. Iwaya, T. Hitosugi, and T. Takahashi, Proc. Natl. Acad. Sci. USA **109**, 19610 (2012).
[17] S.-L. Yang, J. A. Sobota, C. A. Howard, C. J. Pickard, M. Hashimoto, D. H. Lu, S.-K. Mo, P. S. Kirchmann, and Z.-X. Shen, Nat. Commun. **5**, 3493 (2014).
[18] S. Heguri, N. Kawade, T. Fujisawa, A. Yamaguchi, A. Sumiyama, K. Tanigaki, and M. Kobayashi, Phys. Rev. Lett. **114**, 247201 (2015).
[19] N. Emery, C. Herold, M. d'Astuto, V. Garcia, Ch. Bellin, J. F. Mareche, P. Lagrange, and G. Loupias, Phys. Rev. Lett. **95**, 087003 (2005).
[20] We used two different light polarizations along the Γ-K (GK) and Γ-M (GM) directions. While the GM polarization does not allow us to observe the folded π^* band near the Γ point,

we can easily see the weak folded π^* band with GM-polarized light. This is the reason why the data taken with GK geometry in Fig. 2 show the folded bands while the folded bands are not seen in the data in Fig. 3, which was taken with the GM geometry.

[21] L. Boeri, G. B. Bachelet, M. Giantomassi, and O. K. Andersen, Phys. Rev. B **76**, 064510 (2007).

[22] R. L. Dubs, S. N. Dixit, and V. McKoy, Phys. Rev. Lett. **54**, 1249 (1985).

[23] J.-H. Park, C. H. Kim, J. W. Rhim, and J. H. Han, Phys. Rev. B **85**, 195401 (2012).

[24] B. Y. Kim, C. H. Kim, P. J. Kim, W. S. Jung, Y. K. Kim, Y. Y. Koh, M. Arita, K. Shimada, H. Namatame, M. Taniguchi, J. Yu, and C. Kim, Phys. Rev. B **85**, 195402 (2012).

[25] H. Okazaki, R. Yoshida, K. Iwai, K. Noami, T. Muro, T. Nakamura, T. Wakita, Y. Muraoka, M. Hirai, F. Tomioka, Y. Takano, A. Takenaka, M. Toyoda, T. Oguchi, and T. Yokoya, Phys. Rev. B **80**, 035420 (2009).

[26] W. S. Jung, C. S. Leem, Chul Kim, S. R. Park, S. Y. Park, B. J. Kim, E. Rotenberg, and C. Kim, Phys. Rev. B **82**, 235105 (2010).

[27] G. Lamura, M. Aurino, G. Cifariello, E. DiGennaro, A. Andreone, N. Emery, C. Hrold, J.-F. March, and P. Lagrange, Phys. Rev. Lett. **96**, 107008 (2006).

[28] M. Calandra and F. Mauri, Phys. Rev. Lett. **95**, 237002 (2005).

[29] J. S. Kim, L. Boeri, J. R. OBrien, F. S. Razavi, and R. K. Kremer, Phys. Rev. Lett. **99**, 027001 (2007).

[30] W. McMillan, Phys. Rev. **167**, 331 (1968).

[31] X. R. Chen, H. Z. Guo, L. C. Cai, and J. Gao, Chin. Phys. Lett. **22**, 1504 (2005).